Supplementary Information (SI) for Materials Chemistry Frontiers.
This journal is © the Partner Organisations 2025

Supporting Information

Dual Blue Fluorescence and Green Phosphorescence of Hybrid Cadmium Halide for Anti-counterfeiting

Qi Wang,[a,b] Jian-Qiang Zhao,[c] Peng-Yao Xuan,[b] Xin-Yuan Li,[b] Zhao-Xi Wang,[b] Hao-Shuo Lu,[b] Xiao-Wu Lei,[b] Zhi-Hong Jing,[*a] Cheng-Yang Yue[*b]

[a]School of Chemistry and Chemical Engineering, Qufu Normal University, Qufu, Shandong, 273165, P. R. China

[b]Research institute of Optoelectronic Functional Materials, School of Chemistry, Chemical Engineer and Materials, Jining University, Qufu, Shandong, 273155, P. R. China

[c]State Key Laboratory of Structural Chemistry, Fujian Institute of Research on the Structure of Matter, Chinese Academy of Sciences, Graduate School of the Chinese Academy of Sciences, Fuzhou, Fujian, 350002, China

Corresponding Author: Zhi-Hong Jing, Cheng-Yang Yue

E-mail: zhhjing@126.com; yuechengyang@126.com

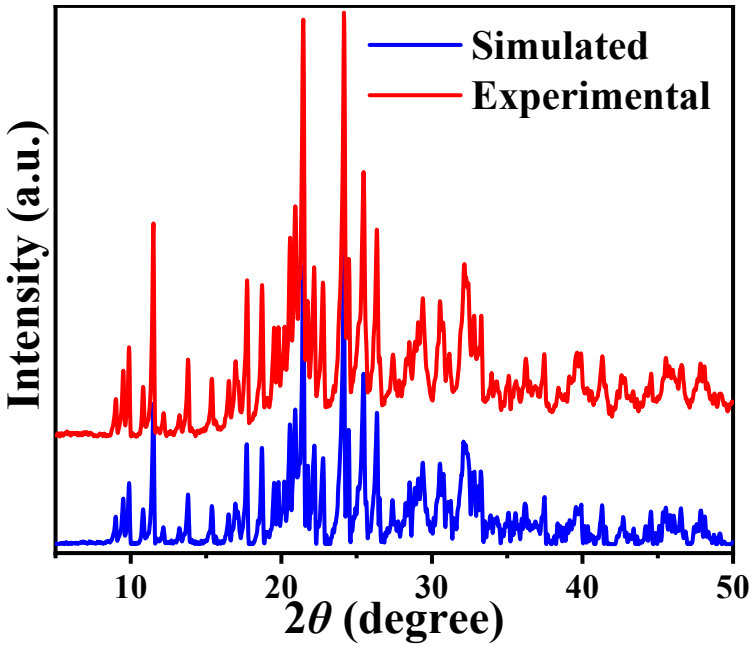

Fig. S1. Experimental and simulated PXRD patterns of [BTPP]Br.

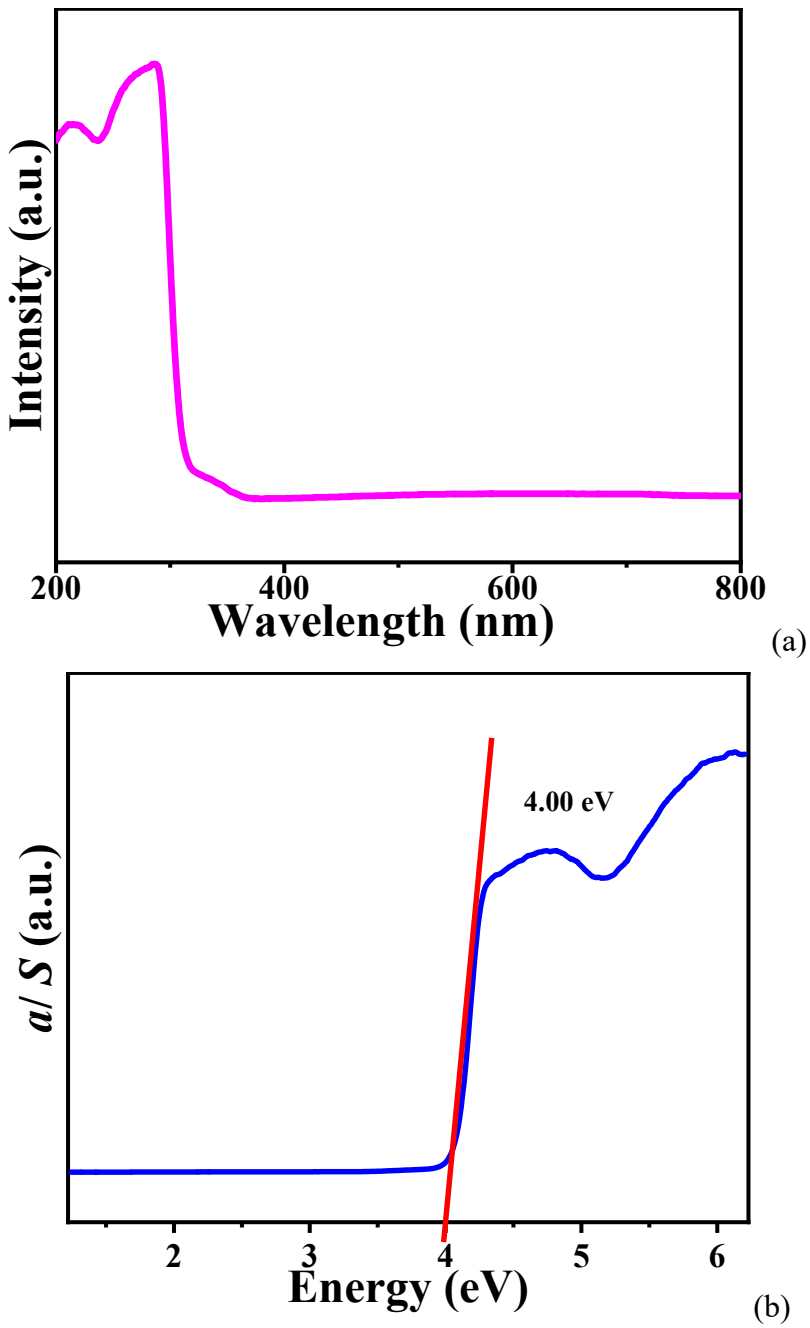

Fig. S2. The solid-state UV-Vis absorption spectra *vs* wavelength (a) and photo energy (b) of [BTPP]Br at 300 K.

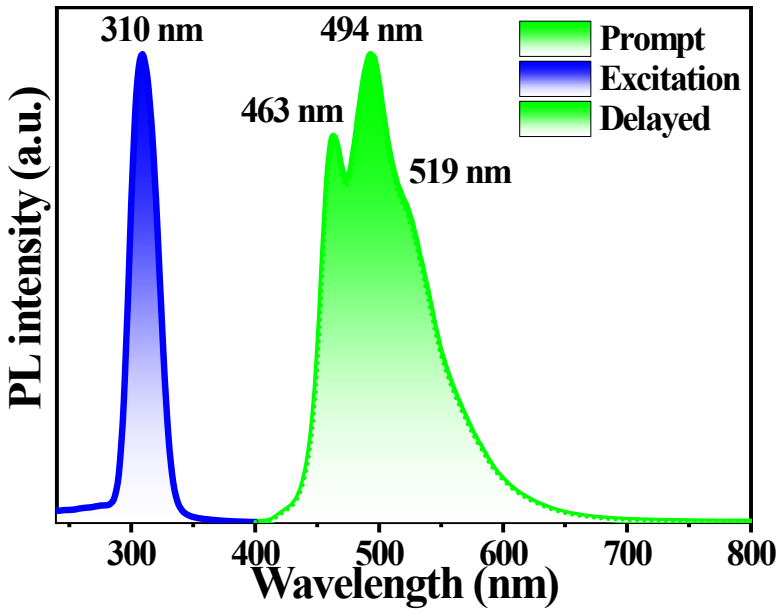

Fig. S3. The PL excitation and emission spectra of [BTPP]Br in prompt- and delayed-mode.

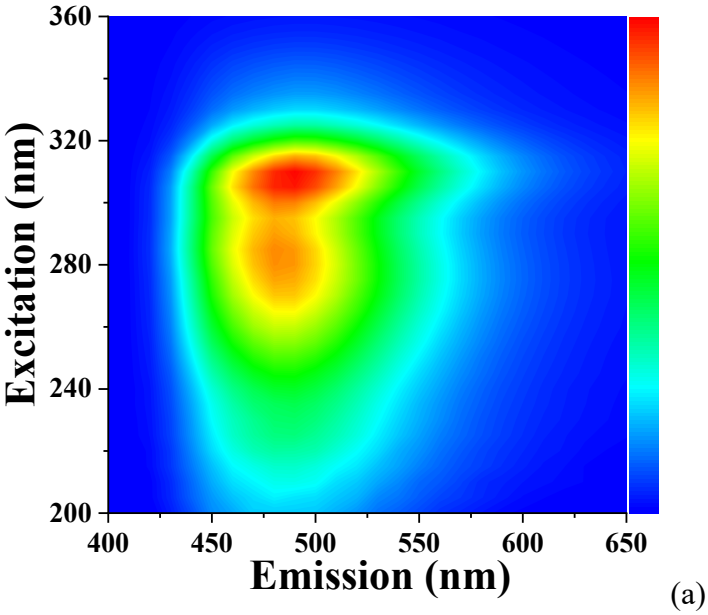

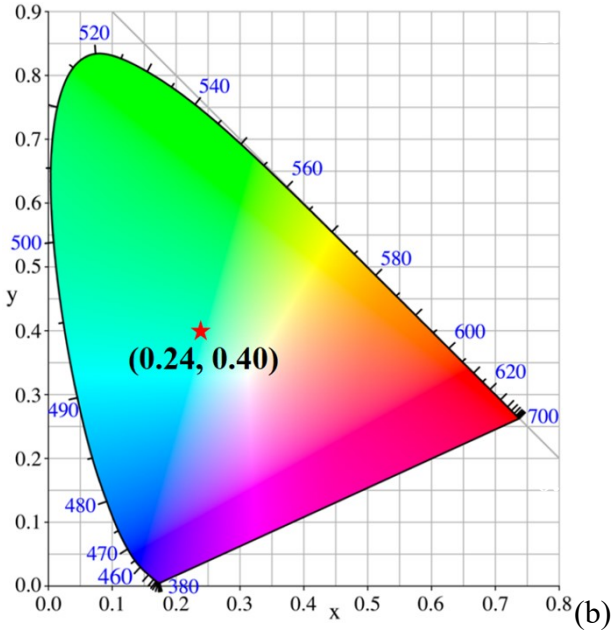

Fig. S4. 3D consecutive PL excitation-emission correlation map (a) and the corresponding CIE coordinates (b) of [BTPP]Br at 300 K.

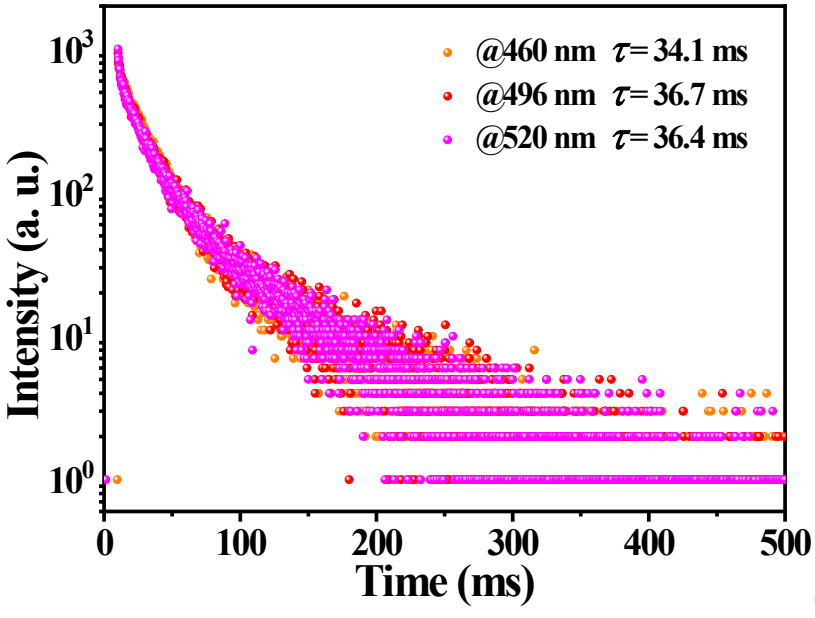

(a)

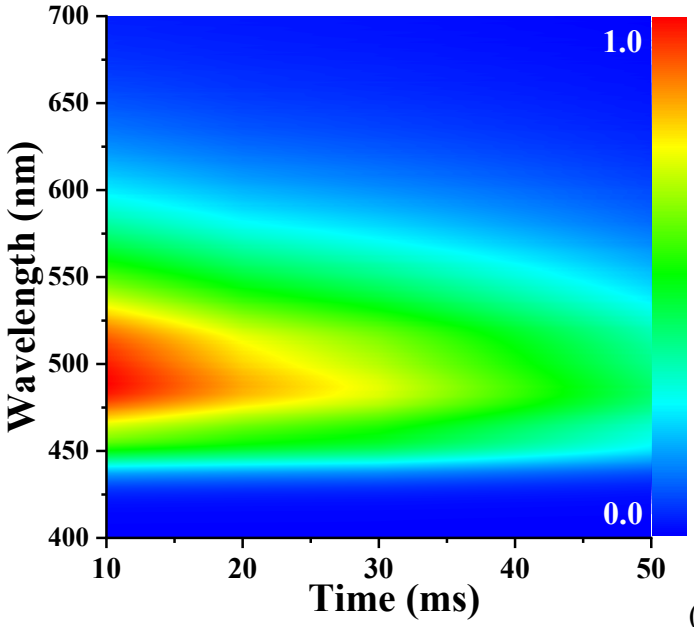

(b)

Fig. S5. The PL decay curves monitoring at 463 nm, 494 nm and 519 nm excited by 310 nm (a), Time-resolved transient emission spectra (b) of [BTPP]Br at 300 K.

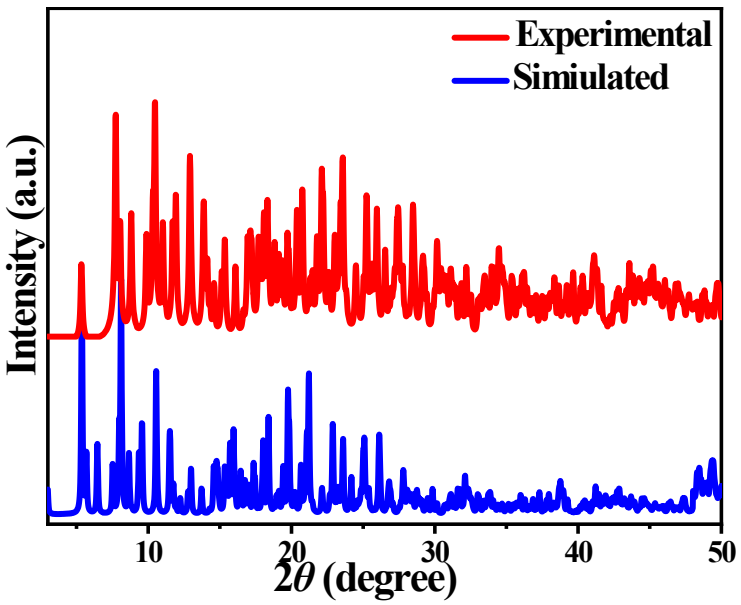

Fig. S6. Experimental and simulated PXRD patterns of $[BTPP]_2CdBr_4$.

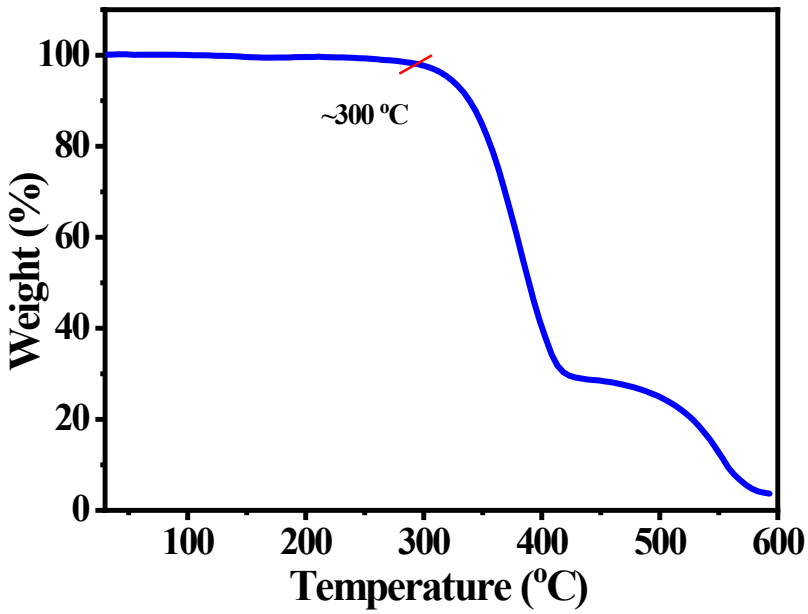

Fig. S7. The thermogravimetric analysis curve of $[BTPP]_2CdBr_4$.

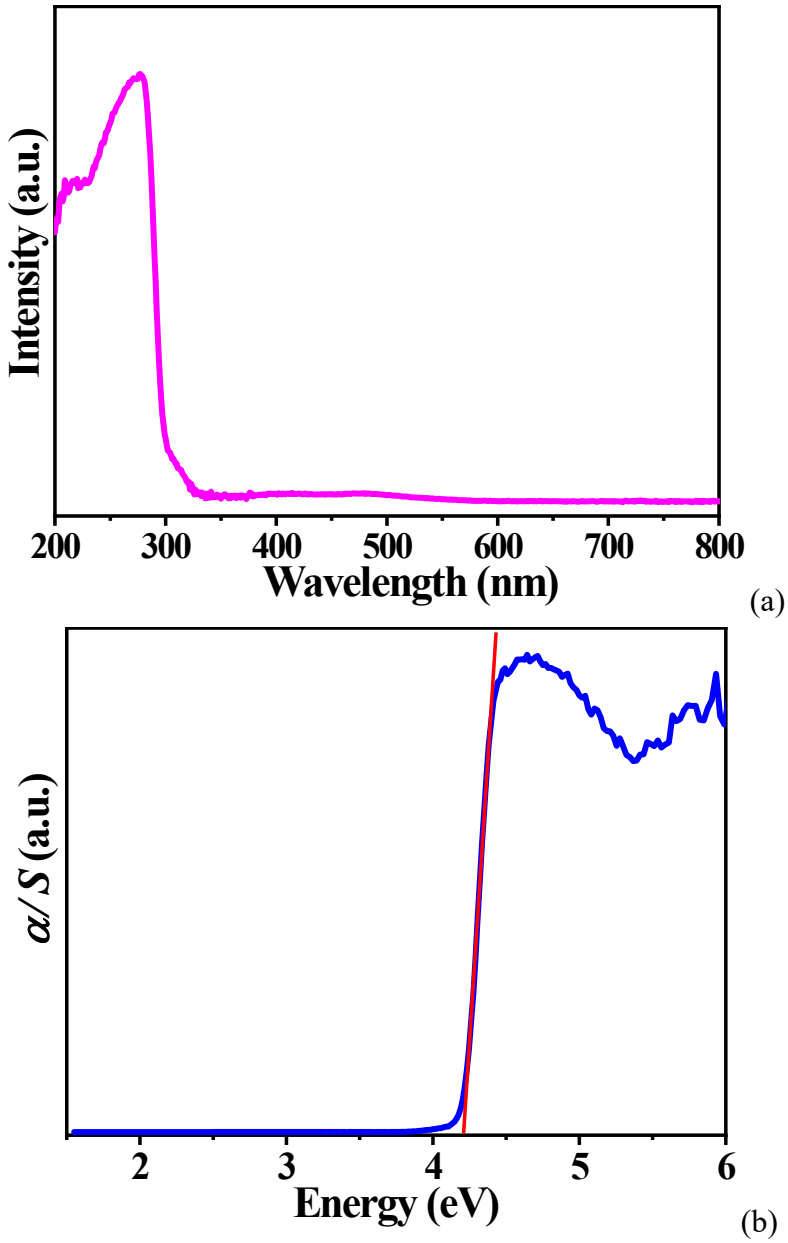

Fig. S8. The solid-state UV-Vis absorption spectra *vs* wavelength (a) and photo energy (b) of $[BTPP]_2CdBr_4$ at 300 K.

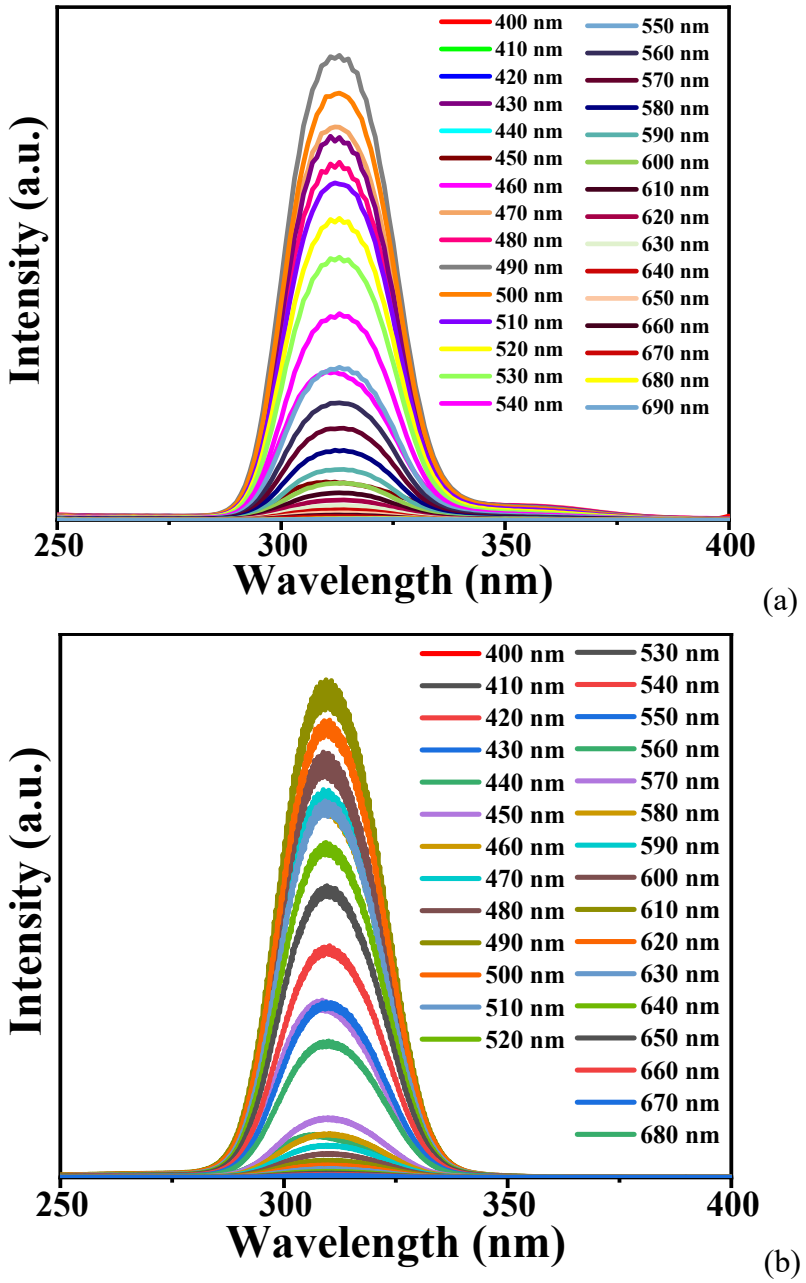

Fig. S9. The prompt-mode (a) and delayed-mode (b) emission wavelength dependent PL excitation spectra of $[BTPP]_2CdBr_4$.

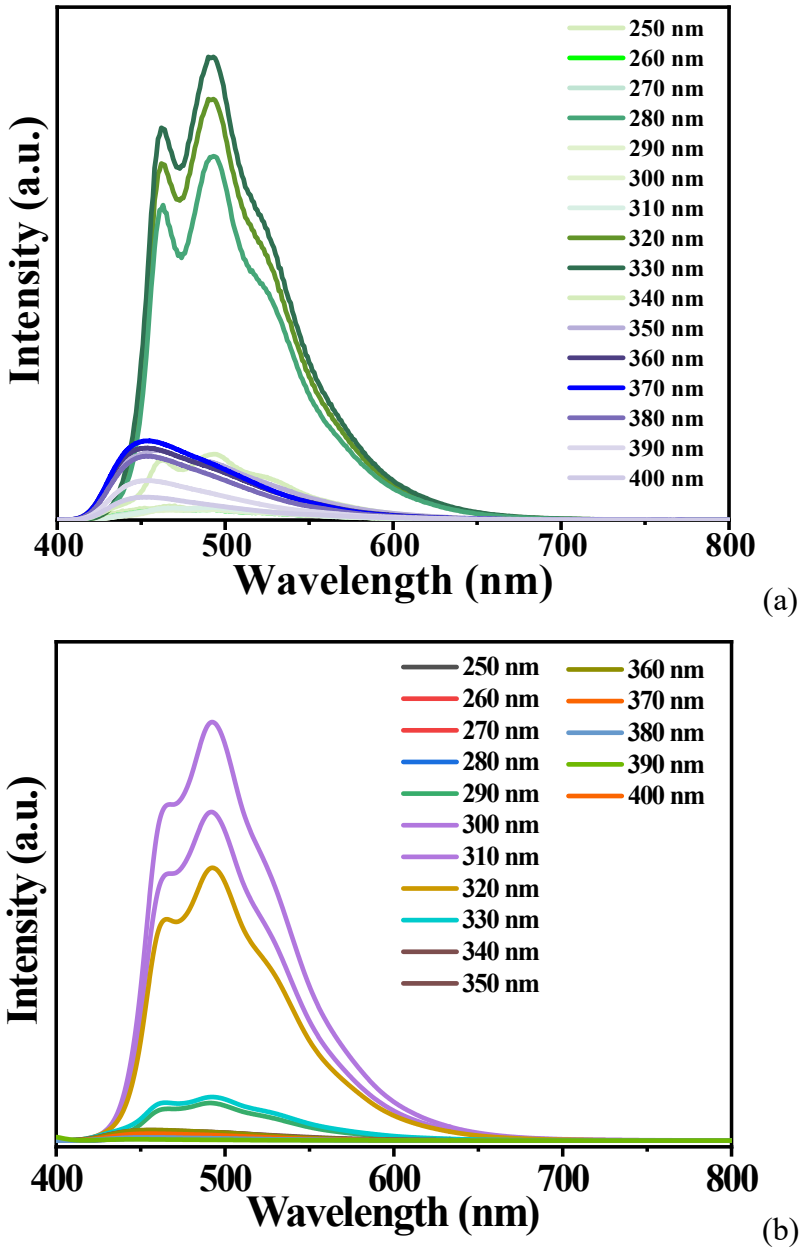

Fig. S10. The prompt-mode (a) and delayed-mode (b) excitation wavelength dependent PL emission spectra of $[BTPP]_2CdBr_4$.

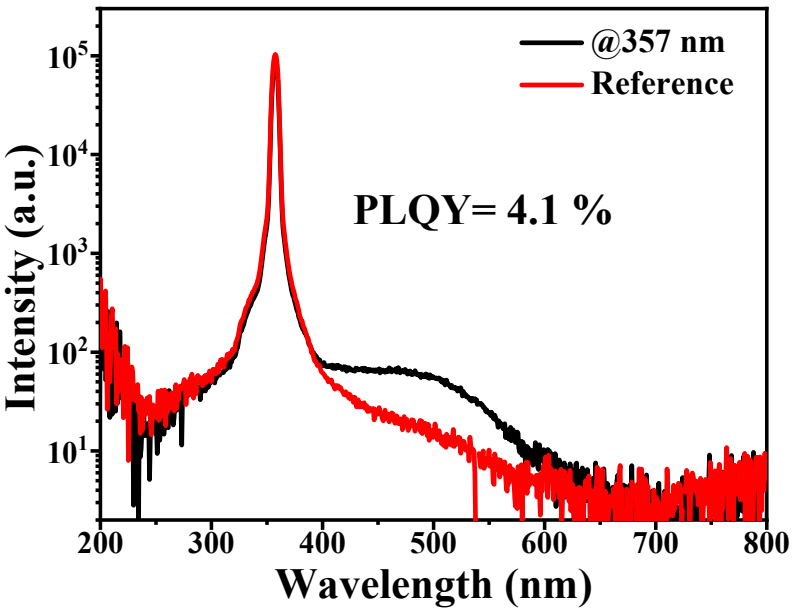

Fig. S11. The PLQY of blue light emission excited by 357 UV light for $[BTPP]_2CdBr_4$ at 300 K.

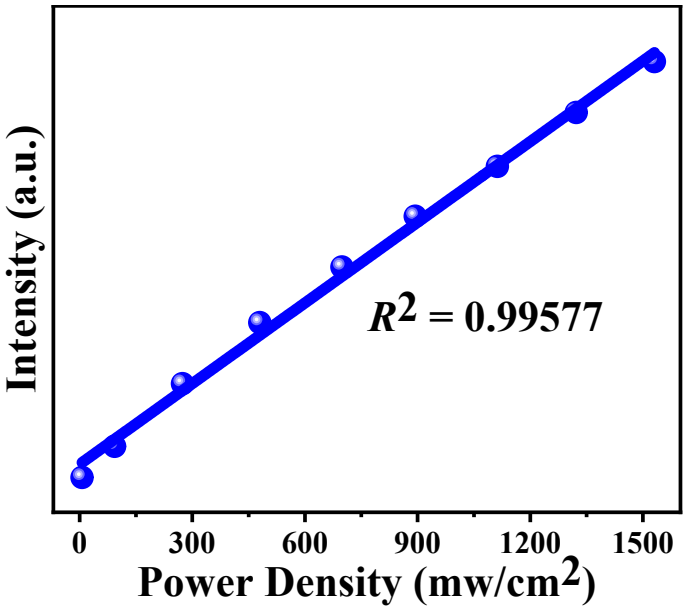

Fig. S12. The power density-dependent luminescence intensity of $[BTPP]_2CdBr_4$.

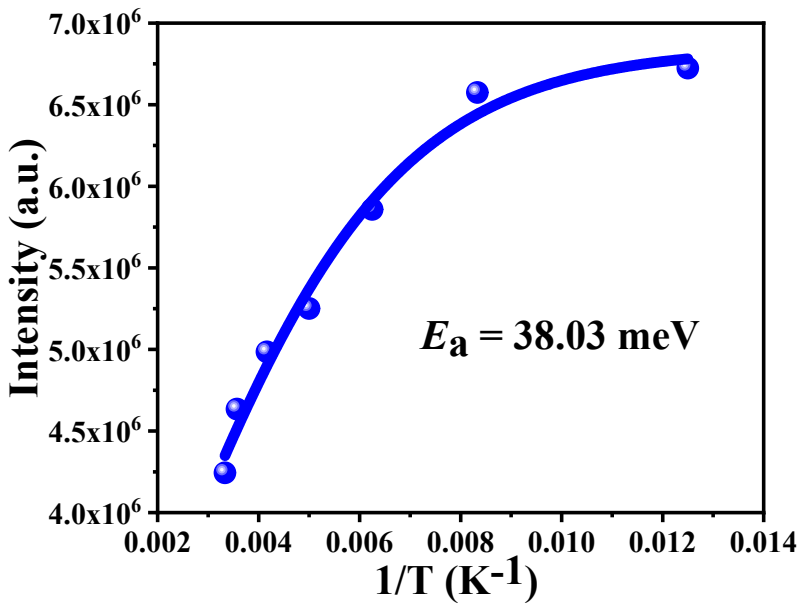

Fig. S13. Integrated PL intensity as a function of reciprocal temperature of $[BTPP]_2CdBr_4$.

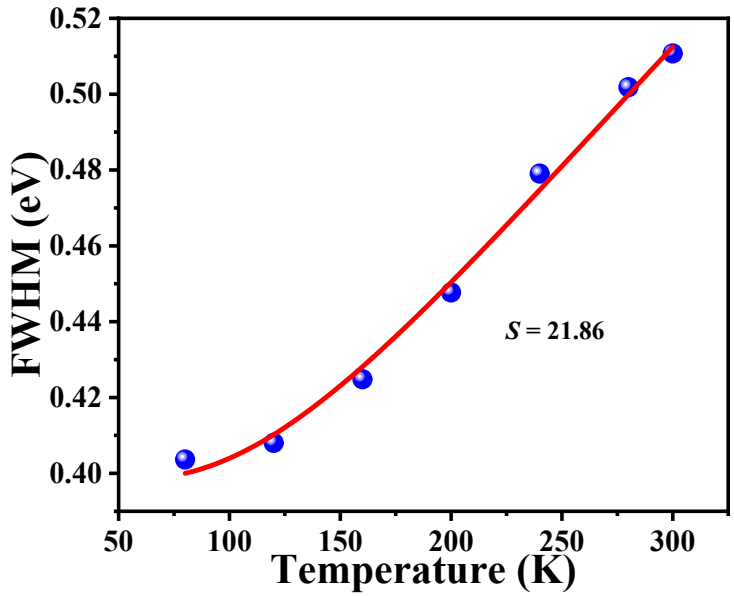

Fig. S14. Experimental and fitted temperature-dependent FWHM of $[BTPP]_2CdBr_4$.

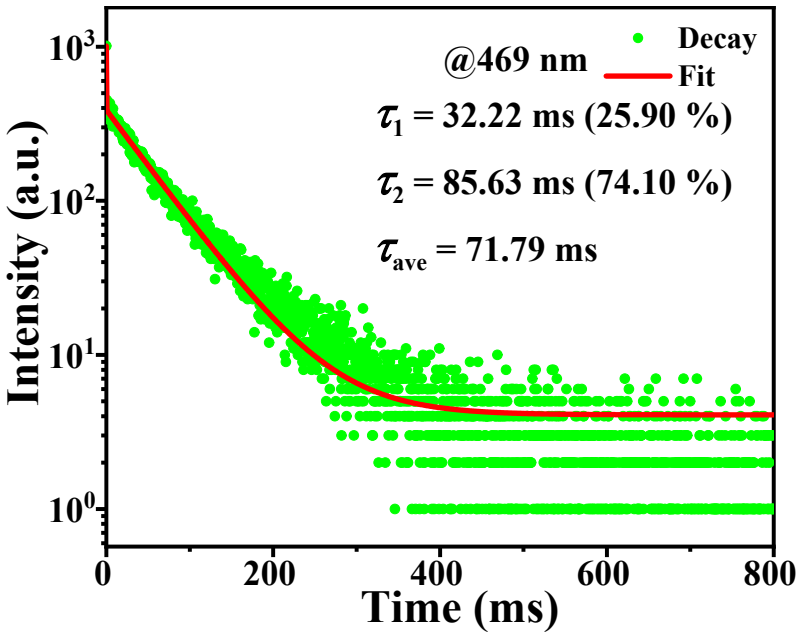

Fig. S15. PL decay curve monitoring at 469 nm excited by 309 nm for $[BTPP]_2CdBr_4$ at 300 K.

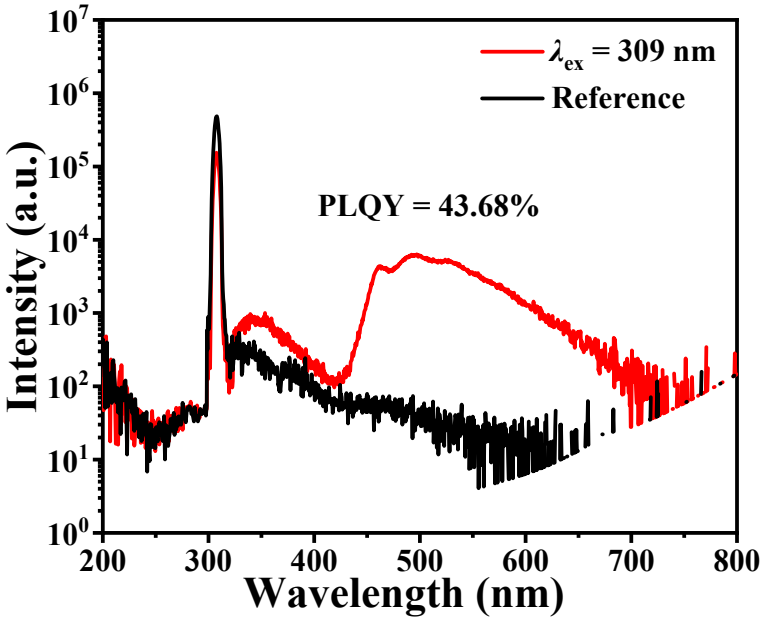

Fig. S16. The PLQY of green afterglow excited by 309 nm UV light for $[BTPP]_2CdBr_4$ at 300 K.

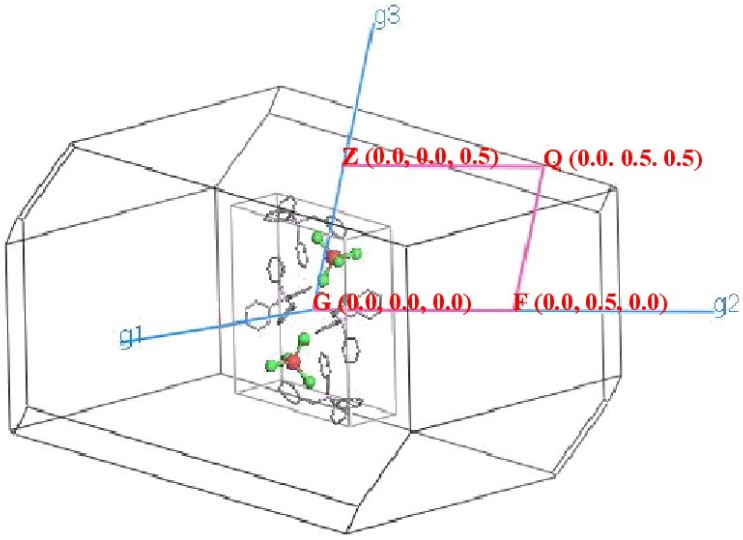

Fig. S17 The high-symmetry *k* points in the Brillouin zone of $[BTPP]_2CdBr_4$.

Table S1. Crystal data and structure refinement for $[BTPP]_2CdBr_4$.

Compound	**$[BTPP]_2CdBr_4$**
chemical formula	$C_{50}P_2H_{44}CdBr_4$
Fw	1138.83
Space group	*P*-1 (No. 1)
a (Å)	10.482(5)
b (Å)	12.470(6)
c (Å)	18.446(8)
α (°)	105.694(1)
β (°)	93.067(2)
γ (°)	92.602(2)
V (Å^3)	2313.3(2)
Z	2
D_{calcd} (g·cm^{-3})	1.635
Temp (*K*)	293
μ (mm^{-1})	4.029
F (000)	1124.0
Reflections collected	52439
GOF on F^2	1.024
$^aR_1$, wR_2 ($I > 2\sigma(I)$)	0.0355/0.0652
$^bR_1$, wR_2 (all data)	0.0703/0.0746

$^aR_1 = \sum ||F_o| - |F_o|| / \sum |F_o|$. $^bwR_2 = [\sum w(F_o^2 - F_c^2)^2 / \sum w(F_o^2)^2]^{1/2}$.

Table S2. Selected bond lengths (Å) and bond angles (°) for $[BTPP]_2CdBr_4$.

Cd1-Br2	2.6460(11)	Cd1-Br4	2.5817(10)
Cd1-Br1	2.5682(9)	Cd1-Br3	2.5713(10)
Br1-Cd1-Br2	111.69(4)	Br4-Cd1-Br2	108.07(2)
Br1-Cd1-Br4	111.62(3)	Br3-Cd1-Br2	105.46(2)
Br1-Cd1-Br3	109.01(3)	Br3-Cd1-Br4	110.82(4)

Table S3. Hydrogen bonds data for $[BTPP]_2CdBr_4$.

D-H···A	**d(D-H)**	**d(H···A)**	**d(D···A)**	**<(DHA)**
C13-H13A···Br2	0.97	2.89	3.847(4)	170
C13-H13B···Br2	0.97	2.88	3.806(4)	161
C24-H24··· Br2	0.93	2.88	3.793(4)	169